Journal of the European Ceramic Society xxx (xxxx) xxx–xxx

Contents lists available at ScienceDirect

Journal of the European Ceramic Society

journal homepage: www.elsevier.com/locate/jeurceramsoc

Original article

Effect of Na-doping on thermoelectric and magnetic performances of textured $Bi_2Sr_2Co_2O_y$ ceramics

G. Çetin Karakaya[a], B. Özçelik[a,*], M.A. Torres[b], M.A. Madre[b], A. Sotelo[b]

[a] Department of Physics, Faculty of Sciences and Letters, Çukurova University, 01330 Adana, Turkey
[b] ICMA (CSIC-Universidad de Zaragoza), C/María de Luna 3, 50018 Zaragoza, Spain

ARTICLE INFO

Keywords:
Thermoelectrics
Laser processing
Seebeck coefficient
Power factor
Figure of merit

ABSTRACT

$Bi_2Sr_{2-x}Na_xCo_2O_x$ (x = 0.0, 0.025, 0.050, 0.075, 0.100, and 0.125) samples were prepared through the solid-state route and textured using the laser floating zone technique. Microstructural analysis of as-grown samples showed well oriented grains and a relatively high amount of secondary phases due to their incongruent melting. Annealing procedure has drastically decreased the number and amount of secondary phases. Moreover, Na-doping has further decreased the secondary phases content and improved grain alignment. These modifications have been reflected in a large decrease of electrical resistivity with the annealing procedure. The maximum power factor values have been obtained in 0.075 Na-doped annealed samples, 0.20 mW/K^{2}m, which are much higher than the best values obtained in textured materials through hot uniaxial pressing. Magnetic properties were very similar for all samples, with paramagnetic Curie temperature and effective magnetic moment values of −48.6 K and ≈2 μ_B, respectively.

1. Introduction

Thermoelectric (TE) materials are characterized by their ability to transform a temperature gradient to electricity without any moving part. As a consequence, they can increase the efficiency of classical energy transforming systems when they are used to recover the wasted heat [1,2]. Moreover, they can be applied as thermoelectric generators [2,3] or heating/cooling devices [2,4,5]. The efficiency of these materials is quantified using the expression $TS^2/\rho\kappa$ (dimensionless figure of merit, ZT), where T, S, ρ, and κ are absolute temperature, Seebeck coefficient, electrical resistivity, and thermal conductivity, respectively [6].

At present, many commercial thermoelectric systems are built using metallic alloys or intermetallic legs, such as Bi_2Te_3 or PbTe which possess high performances at relatively low temperatures [7–9]. Consequently, the high-temperature wasted heat cannot be harvested using these systems. Moreover, they can be degraded and/or release toxic or heavy elements when working in these conditions under air. The possibility to use materials working at high temperatures was reported in 1997, when discovering attractive thermoelectric properties in $NaCo_2O_4$ ceramics [10]. This finding boosted the research on different CoO-based thermoelectric ceramics, as $Ca_3Co_4O_9$ (349), $LaCoO_3$, or $Bi_2AE_2Co_2O_x$ (AE = Alkaline earth) [11–15], with p-type behavior. On the other hand, the study of transition metal oxide systems led to other compounds, as TiO- and MnO-based materials [16,17], which showed n-type behavior and can be used as the p-type counterpart in the thermoelectric modules.

The crystalline structure of these CoO families can be described as a monoclinic structure formed, in turn, by an alternate stacking of two layers: a conductive CoO_2 layer with CdI_2-structure and a rock-salt-type block one. These two layers possess common *a*- and *c*-axis lattice parameters and *β* angles but different *b*-axis length, leading to a misfit structure along the *b*-direction [18,19]. Consequently, the grains possess a large crystallographic anisotropy, reflected in the anisotropy of their electrical properties. As it is well known, the misfit factor and the charge in the rock-salt layer, influence the Seebeck coefficient values [20]. These characteristics have to be considered when tuning up their thermoelectric properties. Following these considerations, many routes have been tested to improve thermoelectric performances, as doping processes [21–25], or texturing techniques [26–30].

The aim of the present work is determining the effect of Na aliovalent substitution for Sr on the microstructure, and thermoelectric performances of laser floating zone (LFZ) textured $Bi_2Sr_2Co_2O_x$ materials.

2. Experimental

Polycrystalline $Bi_2Sr_{2-x}Na_xCo_2O_x$ (x = 0, 0.025, 0.05, 0.075, 0.10,

* Corresponding author.
E-mail address: ozcelik@cu.edu.tr (B. Özçelik).

http://dx.doi.org/10.1016/j.jeurceramsoc.2017.09.006
Received 6 June 2017; Received in revised form 1 September 2017; Accepted 3 September 2017

and 0.125) ceramic precursors have been prepared through the classical solid state method, using Bi_2O_3 (99%, Panreac), $SrCO_3$ (99%, Panreac), Na_2CO_3 (99%, Panreac), and CoO (99.99%, Aldrich) commercial powders as starting materials. They were weighed in the appropriate proportions, mixed, and ball milled for 30 min at 300 rpm in water media. The suspension was totally dried under infrared radiation and the powder was manually milled to break the agglomerates. The homogeneous mixture has been heated twice, at 750 and 800 °C, for about 12 h under air, with an intermediate manual milling, to decompose Na, and Sr carbonates. This process is necessary to avoid their decomposition during the texturing process, otherwise they would produce CO_2 bubbles inside the melt, leading to the crystallization front destabilization [31]. After the thermal treatments, the powders were cold isostatically pressed at ~200 MPa to obtain green ceramic cylinders (ϕ = 2–3 mm and 100 mm length). These cylindrical precursors were subsequently used as feed in a LFZ device equipped with a continuous power Nd:YAG laser (λ = 1064 nm) [32]. All samples have been directionally grown at 30 mm/h, and subjected to 3 rpm seed rotation to maintain the cylindrical geometry. Moreover, an opposite feed rotation of 15 rpm has been used to improve the cations distribution in the molten zone. After the texturing process, geometrically homogeneous textured cylindrical rods (~2 mm diameter) have been obtained. As it has been previously reported, these materials melt incongruently and are composed by a large number of secondary phases [33]. Therefore, some of the as-grown samples were annealed at 810 °C for 24 h with a final furnace cooling to maximize the thermoelectric phase content.

Phases identification was performed through powder X-ray diffraction (XRD) analysis using a Rigaku D/max-B X-ray powder diffractometer (CuKα radiation), between 10 and 60°. Microstructural evolution has been studied on polished longitudinal sections of as-grown and annealed samples in a field emission scanning electron microscope (FESEM, Zeiss Merlin). Qualitative chemical composition has been determined through energy dispersive X-ray spectroscopy (EDS). Moreover, density of samples has been quantified using Archimedes method, and 6.8 g/cm^3 as theoretical density [34].

Electrical resistivity and Seebeck coefficient were determined by the standard dc four-probe technique in a LSR-3 measurement system (Linseis GmbH) between 50 and 650 °C. With these data, power factor (PF = S^2/ρ) has been calculated to determine the samples performances. The magnetic properties were measured in a physical property measurement system PPMS system (Dyne-cool PPMS, Quantum Design) magnetometer. The magnetic hysteresis data have been obtained between − 4 and 4 T external applied fields, and magnetization measurements have been made under 20 Oe dc external field between 5 K and room temperature, in zero field cooled (ZFC) mode.

3. Results and discussion

Powder XRD patterns (from 10 to 40°, for clarity) of representative as-grown and annealed samples are displayed in Fig. 1. In the graph, the diffraction planes indicate the peaks associated to the thermoelectric phase, in agreement with previously published data [35]. Moreover, as it can be clearly observed in Fig. 1a, and b, as-grown samples possess several secondary phases, identified using the peaks marked with *, + and # in Fig. 1a ($Bi_{0.75}Sr_{0.25}O_y$ [36], Sr-rich Bi-Sr-Co-O [37], and Co oxide [38], respectively). When comparing these two patterns, it is easy to deduce that Na-doping decreases the amount of secondary phases, when compared with the undoped ones. On the other hand, when observing Fig. 1c–e, it is clear that annealing procedure drastically reduces the amount of secondary phases (from the as-grown ones), leading to nearly single phase materials. Another important feature observed in these patterns is that the most intense peaks correspond to the ab planes. This effect is associated to the grains shape (thin and large plate-like grains) [38], which tend to be preferentially oriented with their ab planes parallel to the sample holder surface during the samples preparation.

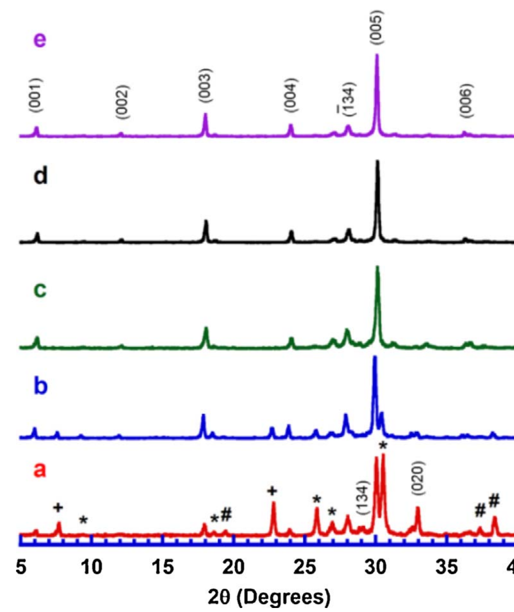

Fig. 1. XRD patterns of representative $Bi_2Sr_{2-x}Na_xCo_2O_y$ as-grown samples with x: a) 0; and b) 0.075; and annealed ones with x: c) 0; d) 0.075; and e) 0.1. Crystallographic planes indicate the peaks corresponding to the thermoelectric phase. *, #, and + correspond to $Bi_{0.75}Sr_{0.25}O_y$, $CoCo_2O_4$, and $Bi_{3.8}Sr_{11.4}Co_8O_{28.875}$ secondary phases, respectively.

Representative FESEM micrographs of longitudinal polished surfaces of as-grown (a, and b) and annealed (c, and d) samples are shown in Fig. 2. The micrographs show several contrasts, indicated by numbers, which correspond to different chemical compositions. These contrasts have been associated, through EDS, to: 1) thermoelectric phase; 2) Co-poor Bi-Sr-Co-O; 3) Bi-Sr-O; 4) Bi-poor Bi-Sr-Co-O; and 5) Co oxide. When comparing undoped and 0.075 Na-doped as-grown samples (Fig. 2a, and b), it is clear that Na-doping decreases the amount of secondary phases, in agreement with the XRD data previously discussed. Moreover, Na-doping leads to a decrease of melting point of samples, reflected in a better grain alignment with respect to the growth direction, due to a lower radial gradient in the solidification front, as observed in similar systems [40]. On the other hand, the effect of annealing can be easily seen when comparing Fig. 2b, and c, corresponding to 0.075 Na doped samples before and after annealing, respectively. As it can be observed in these pictures, annealing decreases the amount and number of secondary phases (#2, and # 4 dissapear). This microstructural evolution evidence that annealing conditions are adequate to promote the TE phase formation from the secondary ones. Moreover, when increasing Na-doping, the secondary phases content still decreases (see Fig. 2c, and d).

Another important feature observed in as-grown and annealed samples (see Fig. 2) is their very low porosity. This is a typical effect of the melt-solidification process when applied to related ceramic systems [41,42]. The high density of these samples has been confirmed through the Archimedes method, reaching 97 ± 2% of the theoretical values in all cases.

The microstructural evolution is clearly reflected in the electrical resistivity displayed in Fig. 3 for as-grown and annealed samples. As it can be observed in the graph, as-grown samples show semiconducting-like behavior ($d\rho/dT < 0$) in the whole measured temperature range, while the annealed possess metallic-like one ($d\rho/dT > 0$). The difference between these two groups of samples can be associated to the larger amount of thermoelectric phase after annealing, and the oxygen content in the thermoelectric phase, which affects the charge carrier concentration. It is well known that LFZ growth promotes the formation of a high number of oxygen vacancies in the textured materials [43], decreasing the charge carrier concentration. On the other hand,